First-principles calculations of carbon clathrates: Comparison to silicon and germanium clathrates

Damien Connétable*

CIRIMAT UMR 5085, CNRS/INP/UPS, Ecole Nationale d'Ingénieurs en Arts Chimiques et Technologiques (ENSIACET) 4, allée Émile Monso, BP 44362, F-31030 Toulouse Cedex 4, France

(Received 19 December 2009; revised manuscript received 18 June 2010; published 26 August 2010)

We employ state-of-the-art first-principles calculations based on density-functional theory and density-functional perturbation theory to investigate relevant physical properties and phase diagram of the free guest type-I (*X*-46) and type-II (*X*-34) carbon clathrates. Their properties and those of silicon and germanium diamonds, and clathrates have been computed and compared within the same approach. We briefly present and discuss their structural, cohesive, and electronic properties. In particular, we present different results about electronic properties of carbon clathrates. From the symmetry analysis of electronic states around the band gap, we deduce their optical properties, and we forecast the effects of hypothetical-doped elements on their electronic band gap. We then report first-principles calculations of vibrational, thermodynamical, and elastic properties. Whereas vibrational properties of Si and Ge systems can be linked through their atomic weight ratio, we show that the vibrational properties of carbon structures differ strongly. Raman and infrared spectra of all clathrates are also calculated and compared. The effects of pressure and temperature on thermodynamical properties (heat capacity, entropy, thermal expansion, etc.) within static and quasiharmonic approximations are investigated. It is shown that thermodynamical properties of carbon clathrates and diamond present a similar evolution up to high pressures (100 GPa) and over a large range of temperatures ([0, 1500] K). Then we deduce the equilibrium phase diagram (P,T) of C-2/C-34/C-46. We conclude the paper with a presentation of elastic properties computed from acoustic slopes.

DOI: 10.1103/PhysRevB.82.075209 PACS number(s): 82.75.−z, 78.30.Na, 63.20.−e, 65.40.De

I. INTRODUCTION

Clathrates have emerged these last decades and have appeared to belong to be a family of compounds with high potentials. The main feature of clathrates is the possibility of tuning their structures: either strongly doped systems (until 20%) or substituted systems. Their properties are then correlated with this tuning: a high thermoelectrical power,[1–4] adapted electronic features (either *n*, *p*, or both type semiconductors in function to the intercalated and substituted elements),[5–8] a large electron-phonon coupling,[9,10] high stability under pressure.[11] Some clathrates present several of these properties: one can cite, for example, the barium or the hypothetical iodine-doped silicon clathrates.[5] Doping elements are changing the carrier concentration in free guest clathrates intrinsic bands and modifying the position of the Fermi level in the system. Similarly, carbon element exists under a large variety of allotropic structures: from three-dimensional (diamond, Si-C, B-C-N alloys, etc.), two-dimensional (graphene, graphite, intercalated graphene), one-dimensional (nanotubes), to zero-dimensional networks (fullerenes, clusters). Each of these structures exhibits actual or potential applications in diverse applied fields.

Carbon clathrates should combine the originality of clathrates (tuning, high doping) with a light element. Due to their speculative existence, the literature on carbon clathrates is not exhaustive. The published studies deal with their lattice parameters,[12–15] bulk modulus, stability, phase diagram,[13,16] electronic band structures,[17,18] plastic features,[19] and about their potential superconductivity.[10,18,20,21] Studies of their fundamental vibrational and associated properties remain nevertheless limited within a full density-functional-theory (DFT) approach. As it has been shown, carbon clathrates should yield large critical temperature and have a hardness similar to diamond. It is also significant to explore any special features in the thermal expansion, heat capacity, Raman, infrared spectra, and phase diagram of these unusual expanded-framework semiconducting crystals.

The purpose of this paper is to present and discuss, by means of a first-principles approach, the properties of two empty carbon clathrates -C-34 and C-46-, and to compare them to other empty clathrates of group IV (Si and Ge). The first part of the manuscript is briefly devoted to the structural, energetic, and electronic properties, which are presented and compared to those of the literature. An analysis of symmetries of electronic states around the band gap of carbon clathrates is in particular displayed. In the second part, using the density-functional perturbative theory, we present the properties calculated from dynamical properties: an analysis of phonon spectra, of Raman and infrared intensities, a study of the effect of temperature and pressure on thermodynamical properties and the (T,P) phase diagram of C-2/C-34/C-46. We conclude by a discussion on their elastic properties.

II. PRESENTATION

Clathrates are composed of polyhedral cages which are sharing their faces. The atoms are linked together through sp^3-type covalent bonds. The nearest-neighbor distances and the angles between bonds are approximately the same as those found in the diamond systems. Their main difference with diamonds is the presence of 87% of pentagonal cycles, where there are only hexagonal cycles. These pentagonal cycles are expected to be at the origin of the specific electronic and dynamical properties of clathrates.[22] Besides, the originality of cagelike materials is the possibility of a huge

TABLE I. Wyckoff positions of type-I and type-II clathrates.

X-34 ($Fd\bar{3}m$: No 227)		X-46 ($Pm\bar{3}n$: No 223)	
8a(2)	x,y,z=0 and =1/4	6c	x=1/4; y=0; z=1/2
32e(8)	x,y,z=−0.092	16i	x,y,z=0.184
96g(24)	x,y=−0.058; z=0.246	24k	x=0; y=0.308; z=0.117

endohedral doping. Clathrates can thus be doped either by inserting (intercalation) until one atom in each cage, which corresponds to 20% of doping, or by substitution. Doping of clathrates is thus much easier than doping of the diamond phase (only some percent by substitution).

The type-I clathrate, namely, X-46, has a simple cubic lattice with 46 atoms per unit cell and the $Pm\bar{3}n$ (No. 223) group symmetry (see Table I). The type-II clathrate, called X-34 or X-136, is a face center cubic lattice with 34 atoms in the unit cell and the $Fd\bar{3}m$ (No. 227) symmetry.

III. THEORETICAL FRAMEWORK

Calculations have been performed using the DFT-based QUANTUM-ESPRESSO package (Ref. 23). The local density approximation, through the Perdew-Zunger parameterization[24] of the Ceperley-Alder exchange correlation functional,[25] and norm-conserving Troullier-Martins[26] pseudopotentials factorized in Kleinman-Bylander form[27] have been employed. To optimize the structures, the Brillouin zone has been sampled by a $2\times2\times2$ Monkhorst-Pack grid[28] which corresponds to one and two irreducible k points for X-46 and X-34, respectively. The wave functions are expanded on plane-wave basis with kinetic energies up to a real-space grid with 50 Ryd (for carbon) and 20 Ryd (for germanium and silicon) energies cutoff. For the electronic density of states (eDOS) and the formation energies, we have adopted finest grids ($10\times10\times10$) with higher energies cutoff (60 Ryd for carbon and 30 Ryd for Si/Ge systems).

The phonon frequencies have been determined by the dynamical matrix, Born effective charges, and dielectric constants, which have been computed using the linear response theory of the DFT.[29,30] In order to generate the force constants matrices and carry out the inverse Fourier transformation, $2\times2\times2$ **q** grids have been employed for static properties (with $6\times6\times6$ **k** grids mesh, and 50 and 20 Ryd of energies cutoff for carbon and silicon/germanium systems, respectively). For diamond phases, we have increased the **k** and **q** grids ($15\times15\times15$ and $8\times8\times8$, respectively). The vibrational density of states has been calculated on $20\times20\times20$ grids with the tetrahedron method.

IV. STRUCTURAL AND ELECTRONIC PROPERTIES

In the Table II we report the optimized lattice parameters, the bulk modulus (fitted by a Murnaghan's equation of state[37]) as well as the cohesive energies of the corresponding species (X=C, Si, and Ge) and crystallographic structures (X-2=diamond, X-34, and X-46). These results are found in good agreement with the experimental data and theoretical

TABLE II. Carbon, silicon, and germanium diamond and clathrates phases lattice parameters (in Å), bulk modulus (in GPa), and formation energy (in meV/atom). The evolution of the atomic volume taken as reference diamond phase δV is given [$\delta V = V_{at}(X\text{-}2)/V_{at}(\text{system})$].

System	a_o	δV	B_o	E_f
C-2	3.58 (3.57[a])	1.00	460 (545[a])	0
C-34	9.60 (9.56[b])	0.86	393 (398[b])	150 (134[c])
C-46	6.65 (6.80[d])	0.87	395 (398[e])	110 (144[c])
Si-2	5.41 (5.43[a])	1.00	97 (99[a])	0
Si-34	14.53 (14.62[f])	0.87	86 (84[g])	60 (80[g])
Si-46	10.08 (10.15[g])	0.88	87 (84[g])	70 (90[g])
Ge-2	5.58 (5.66[a])	1.00	75 (77[a])	0
Ge-34	15.02 (15.13[h], 15.21[i])	0.88	68 (67[j], 61[h])	40 (50[h])
Ge-46	10.40 (10.47[h])	0.89	68 (68[j], 62[h])	50 (50[h])

[a]Reference 31.
[b]Reference 17.
[c]Reference 12.
[d]Reference 20.
[e]Reference 19.
[f]Reference 32.
[g]Reference 33.
[h]Reference 34.
[i]Reference 35.
[j]Reference 36.

predictions for the germanium (see Refs. 34 and 36), silicon (Refs. 12, 22, 32, and 33), and carbon elements (Refs. 12–14, 17, 19, and 20).

The electronic band structures (eBS) and eDOS of carbon and silicon systems are plotted in Fig. 1 (electronic properties of germanium clathrates are not presented here). We found that all empty clathrates are semiconductors with a large gap. Band gaps (Δ_{gap}, Table III) are found greater in Ge/Si clathrates than in diamond phases, contrary to carbon clathrate, in agreement with previous DFT values.[17,32,36]

We provide a qualitative interpretation of the variation in this electronic band gap for silicon and carbon elements (the case of germanium is different due to the presence of d core states): from chemical and crystallographic arguments. Gaps in Γ are found smaller in clathrates than in diamonds. Since

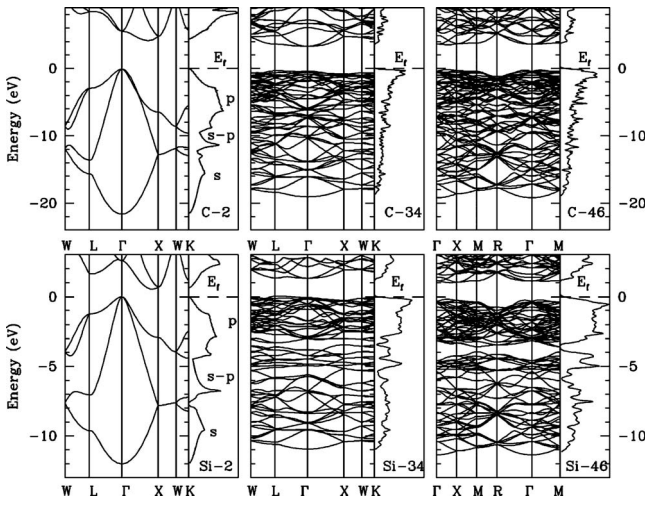

FIG. 1. Electronic band structures (in eV) and density of states. The Fermi level has been put at the top of the valance band.

TABLE III. Band gaps (Δ_{gap}) in eV.

C-2	C-34	C-46
3.9 (5.48[a])	3.7 (5.15[b])	3.7 (5.25[b])
Si-2	Si-34	Si-46
0.62 (1.17[a])	1.25 (1.85[b], 1.9[d])	1.3 (1.9[b])
Ge-2	Ge-34	Ge-46
0.34 (0.74[a])	0.95 (0.80[c])	1.4 (1.46[e], 1.31[c])

[a]Experiment (Ref. 31).
[b]GW simulations (Refs. 17 and 18).
[c]DFT simulation (Ref. 36).
[d]Experiment (Ref. 38).
[e]DFT simulation (Ref. 39).

clathrates are highly isotropic systems comparatively to the diamond, the dispersion of the electronic bands is weak outside Γ (flat bands). Moreover, in the case of carbon, shells are less sensitive than silicon to the crystallographic environment (no internal *p* shells, and the system is more compact), the band gap is smaller in carbon clathrates than in diamond. Contrarily, silicon is more affected by its crystallographic environment and the band gap is then reduced in diamond.

For sake of completeness, the irreducible representation of electronic states around band gaps have been analyzed, as already done for silicon clathrates.[8] For a given structure, the symmetries are found to be roughly the same for carbon and silicon clathrates: along different crystallographic directions, the states of the bottom of conduction bands and the top of valence bands have the same symmetries (see Table IV at Γ). Only some states, near the top of the valence bands, change. From these results and from our previous analysis of silicon clathrates, we deduce that, for carbon clathrates, the optical transitions should be forbidden by means of symmetries in a dipole approximation. Furthermore, the effect of doped elements on electronic properties of carbon clathrates can be forecast by symmetry. Only the bottom of the conduction states should be hybridized by states of the intercalated element. So, the electronic gap should be increased like in silicon clathrates.

TABLE IV. Symmetry classification of the valence and conduction bands around the electronic band gap for *X*-46 and *X*-34 systems where *X*=Si and C. The energies (in eV) are calculated at the **Γ** point (symmetry O_h). The reference energies have been set at the top of the valence bands in the **Γ** point.

	C-46	Si-46
E_{v3}	−0.19(E_u)	−0.11(E_u)
E_{v2}	−0.05(T_{1g})	−0.10(T_{2g})
E_{v1}	0.00 (A_{1u})	0.00 (A_{1u})
E_{c1}	+4.06(T_{1u})	+1.45(T_{1u})
E_{c2}	+5.34(A_{2g})	+1.82(A_{2g})
	C-34	Si-34
E_{v3}	−0.43(T_{2u})	−0.10(T_{2u})
E_{v2}	−0.17(T_{1g})	−0.01(E_u)
E_{v1}	0.00 (E_u)	0.00 (T_{1g})
E_{c1}	+3.63(T_{1u})	+1.46(T_{1u})
E_{c2}	+6.40(A_{2u})	+2.22(A_{2u})

V. DYNAMICAL PROPERTIES

A. Vibrational properties

1. Phonon dispersion curves

Our results for the phonon-dispersion curves (*v*band) of diamond and clathrates (C, Si, and Ge elements) along several symmetry lines together with the corresponding vibrational density of states (*v*DOS) are displayed Fig. 2. Numerical values at the **Γ** point are listed in Tables V and VI for *X*-34 and *X*-46 clathrates, respectively, and compared with literature data. The vibrational spectra of diamond phases—not reported here—are in agreement with experimental data (discrepancy in frequencies less 1%). According to the O_h group symmetry and the Wyckoff positions of atoms in the network (see Table I), the symmetry of the vibrations (noted *v*SM) are the following:

$$\begin{cases} \boldsymbol{v}\mathbf{SM}_{6c} = A_{2g} \oplus E_g \oplus T_{1g} \oplus T_{2g} \oplus T_{1u} \oplus T_{2u} \\ \boldsymbol{v}\mathbf{SM}_{16i} = A_{2g} \oplus A_{1g} \oplus 2E_g \oplus 3T_{1g} \oplus 3T_{2g} \oplus \\ \quad A_{1u} \oplus A_{2u} \oplus 2E_u \oplus 3T_{1u} \oplus 3T_{2u} \\ \boldsymbol{v}\mathbf{SM}_{24k} = 2A_{2g} \oplus 2A_{1g} \oplus 4E_g \oplus 4T_{1g} \oplus 4T_{2g} \\ \quad \oplus A_{1u} \oplus A_{2u} \oplus 2E_u \oplus 5T_{1u} \oplus 5T_{2u} \end{cases} \quad (1)$$

for *X*-46 and for *X*-34

$$\begin{cases} \boldsymbol{v}\mathbf{SM}_{8a} = T_{1u} \oplus T_{2g} \\ \boldsymbol{v}\mathbf{SM}_{32e} = A_{1g} \oplus A_{2u} \oplus E_g \oplus E_u \oplus T_{1g} \oplus 2T_{1u} \\ \quad \oplus 2T_{2g} \oplus T_{2u} \\ \boldsymbol{v}\mathbf{SM}_{96g} = 2A_{1g} \oplus A_{1u} \oplus A_{2g} \oplus 2A_{2u} \oplus 3E_g \oplus \\ \quad 3E_u \oplus 4T_{1g} \oplus 5T_{1u} \oplus 5T_{2g} \oplus 4T_{2u} \end{cases} \quad (2)$$

From selections rules[43] and the knowledge of symmetries, we have forecast the Raman and infrared frequencies (noted in the tables *R* and *IR*, respectively). The group theory assumes that, for cubic systems belonging to the O_h group symmetry, the A_{1g}, E_g, and T_{2g} irreducible representations could be Raman active while the infrared modes should have the T_{1u} symmetry.

For carbon clathrates, no theoretical values have been reported, except for the frequencies of active Raman modes in the hypothetical lithium-doped clathrate.[16] In the case of other elements, theoretical frequencies have been already calculated (see values reported in Tables V and VI). Raman measurements have been only done in the case of Si-34.[40,41,44] Our results are in excellent agreement with those of the literature.

We note that the vibrational dispersion curves for Si and Ge clathrate are very close, while *v*band and *v*DOS of carbon clathrates differ significantly from these systems. The difference between Si and Ge systems can be rationalized using their respective atomic weights,[45] as already mentioned for diamond.[46] The interatomic forces of C-34 and C-46 clathrates are different from the other clathrates in spite of a similar sp^3 hybridization.

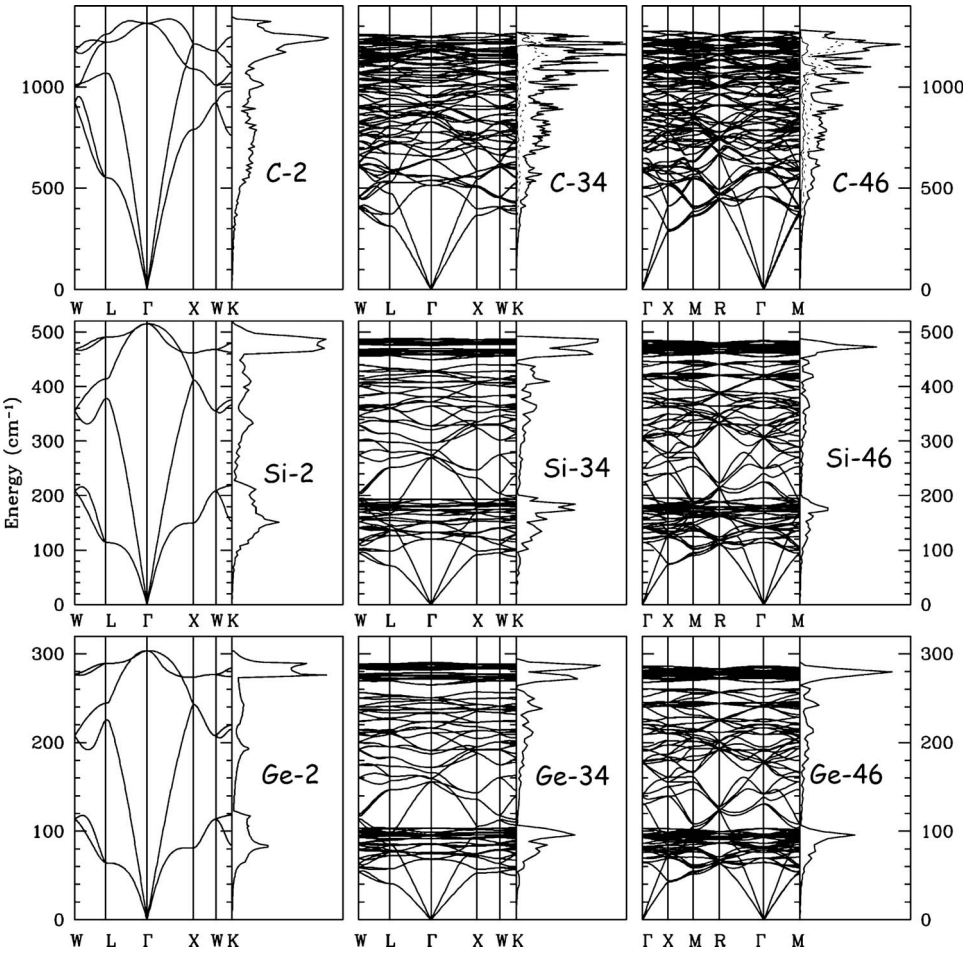

FIG. 2. Vibrational band structures (in cm^{-1}) and density of states. We also report the contribution of atoms in $6c/16i$ and $8a/32e$ Wyckoff positions for C-46 and C-34, respectively, in thin lines and dashed lines.

In carbon clathrates, the transverse acoustic modes are no longer flat unlike in other Si/Ge systems, which explain why the sharp features of the vDOS (subband) are lacking. As in Si/Ge clathrates, most of tetrahedral semiconductors display a peculiar flatness in the transverse acoustic frequencies region (these bands are correlated with long range of inter atomic forces).[46] In diamond, this difference is less tagged due to its higher compacity.

A comparative analysis of the frequencies in diamond and clathrates reveals that there is in C-34/C-46 two "redshifts" (for optical and acoustic modes) and one "blueshift" in acoustic modes and one "redshift" in optical modes in Si/Ge clathrates. The redshift is associated with the weakening of the *X*-*X* bonds between clathrates and diamonds. The frustration of the optical modes, due to the presence of pentagonal cycles, induces this shift of 40 cm^{-1} toward low frequencies in C-34/C-46 and Si/Ge clathrates. The number of optical modes, associated with the asymmetric vibrations of two neighbors atoms, decreases with the frustration. We can also note a gap in Si/Ge optical frequencies. This gap does not exist in carbon clathrates. The maximum of the optical branches is not located at the zone center for both C-34 and C-46 as in carbon diamond, contrary to other systems, which results in sharp peaks in vDOS for C-34, C-2 and—but less pronounced–for C-46. It is due to the overbending of the optical branches and has been associated, in diamond,[47] to a sufficiently large interatomic force constants between second-nearest neighbor.

2. Raman shifts

Following Ref. 48, the Raman tensor and Raman spectra have been calculated from first-principles approaches. Raman intensities are plotted on Figs. 3 and 4 for type-I and type-II clathrates, respectively. The Raman cross section (at the bottom) is convoluted with a Gaussian broadening and the Raman total intensities of powders are determined following Ref. 49 (Lorentzian convolution). A 10 cm^{-1} is used as damping constants. The parallel and perpendicular Raman intensities to the incident polarization have been calculated from the depolarization ratio ρ_r ($\rho_r=3/4$ for E_g and T_{1g}, and $\rho_r=0$ for A_{1g}) and added on Figs. 3 and 4.

As already mentioned, only the Raman spectrum of the free guest Si-34 has been investigated experimentally.[40,41,44] Raman spectra has been calculated for Si-34 by Dong[50] and Ge-34/Ge-46 (Ref. 34) using a bond-polarizability model. In Ge systems, the peaks are located at the same positions (shifted, around 10 cm^{-1} different). In Si-34, three peaks are observed around 120, 250–300, and 470 cm^{-1}, as claimed by Guyot.[44] The calculated spectra is similar to the experimental spectra obtained by Tang *et al.*[41] and Nolas *et al.*[40] However, some peaks are missing: in Tang measurements, one A_{1g} mode at around 320 cm^{-1}, one T_{2g} mode at 467 cm^{-1}, or in Nolas measurements, the E_g and A_{1g} modes at 454 cm^{-1} and 480 cm^{-1}, respectively, what makes the comparison sometimes difficult. For example, we arrive to reproduce the vanishing of the A_{1g} mode in parallel polarized Stokes Ra-

TABLE V. Frequencies (in cm^{-1}) and symmetries of the vibrational modes in $\mathbf{\Gamma}$ for *X*-34.

C-34		Si-34				Ge-34			
$\omega_{q,\nu}$	Sym.	$\omega_{q,\nu}$	Sym.	Expt. (Refs. 40 and 41)		$\omega_{q,\nu}$	Sym.	Theo. (Ref. 34)	
0	T_{1u}^{IR}	0	T_{1u}^{IR}			0	T_{1u}^{IR}	0	T_{1u}^{IR}
513	T_{2g}^{R}	119	T_{2g}^{R}	117/120	T_{2g}^{R}	69	T_{2g}^{R}	54	T_{2g}^{R}
538	E_{g}^{R}	131	T_{1g}			76	T_{1g}	72	T_{1g}
562	T_{1g}	133	E_{g}^{R}	130/133	E_{g}^{R}	77	E_{g}^{R}	74	E_{g}^{R}
641	T_{1g}	149	T_{2u}			86	T_{2u}	79	T_{1u}^{IR}
657	T_{2u}	154	T_{1g}			87	T_{1g}	81	T_{2u}
690	E_{u}	163	E_{u}			93	E_{u}	81	T_{1g}
721	T_{1u}^{IR}	171	T_{1u}^{IR}			95	T_{2u}	84	T_{2g}^{R}
776	T_{2u}	174	T_{2u}			96	T_{1u}^{IR}	88	E_{u}
827	T_{2g}^{R}	177	T_{1g}			96	T_{2g}^{R}	90	T_{1g}
847	T_{1u}^{IR}	180	T_{2g}^{R}	184/165	T_{2g}^{R}	97	T_{1g}	91	T_{2u}
863	T_{1u}^{IR}	181	A_{2g}			98	A_{2g}	93	A_{2g}
869	T_{1g}	194	T_{1u}^{IR}			104	T_{1u}^{IR}	97	T_{1u}^{IR}
874	A_{2u}	268	T_{1u}^{IR}			156	T_{1u}^{IR}	154	T_{1u}^{IR}
894	A_{1g}^{R}	270	T_{2g}^{R}	271/272	T_{2g}^{R}	159	T_{2g}^{R}	157	T_{2g}^{R}
906	A_{2g}	283	A_{2u}			166	A_{2u}	162	A_{2u}
913	T_{2g}^{R}	294	E_{u}			173	E_{u}	170	E_{u}
927	E_{u}	318	A_{1g}^{R}	(316)/320	A_{1g}^{R}	187	A_{1g}^{R}	180	A_{1g}^{R}
947	T_{2g}^{R}	326	T_{2g}^{R}	324/333	T_{2g}^{R}	191	T_{2g}^{R}	187	T_{2g}^{R}
958	E_{g}^{R}	362	E_{g}^{R}	360/362	E_{g}^{R}	211	E_{g}^{R}	205	E_{g}^{R}
1003	T_{2g}^{R}	368	T_{2u}			216	T_{2u}	210	T_{2u}
1020	A_{2u}	381	T_{1u}^{IR}			223	T_{1u}^{IR}	218	T_{1u}^{IR}
1032	A_{1g}^{R}	397	A_{2u}			233	A_{1g}^{R}	225	A_{2u}
1046	T_{1u}^{IR}	397	A_{1g}^{R}	387/383	A_{1g}^{R}	234	A_{2u}	227	A_{1g}^{R}
1056	E_{u}	405	T_{2g}^{R}	401/404	T_{2g}^{R}	237	T_{2g}^{R}	234	T_{2g}^{R}
1076	T_{2u}	416	A_{2u}			244	A_{2u}	236	A_{2u}
1094	T_{1g}	421	T_{1g}			246	T_{1g}	243	T_{1g}
1107	A_{1u}	427	T_{1u}^{IR}			250	T_{1u}^{IR}	248	T_{1u}^{IR}
1114	T_{1u}^{IR}	447	E_{u}			265	E_{u}	261	E_{u}
1137	E_{g}^{R}	456	A_{1g}^{R}	454/	A_{1g}^{R}	271	T_{2u}	268	T_{2u}
1145	T_{2u}	456	T_{2u}			272	A_{1g}^{R}	269	T_{1u}^{IR}
1171	A_{2u}	460	T_{1u}^{IR}			273	T_{1u}^{IR}	270	A_{1g}^{R}
1175	T_{2g}^{R}	462	E_{u}			275	E_{u}	271	E_{u}
1181	T_{2u}	463	E_{g}^{R}	466/454	E_{g}^{R}	276	E_{g}^{R}	273	E_{g}^{R}
1189	A_{1g}^{R}	468	T_{2g}^{R}	/467	T_{2g}^{R}	279	T_{2g}^{R}	274	T_{2g}^{R}
1198	T_{1u}^{IR}	473	T_{2g}^{R}	472/471	T_{2g}^{R}	282	T_{2g}^{R}	275	T_{1u}^{IR}
1200	T_{2g}^{R}	475	T_{1u}^{IR}			283	T_{1g}	276	T_{2g}^{R}
1204	E_{u}	475	T_{1g}			284	T_{1u}^{IR}	279	T_{1g}
1218	T_{1u}^{IR}	478	A_{1u}			285	A_{1u}	281	T_{2g}^{R}
1227	T_{1g}	482	E_{g}^{R}	480/	E_{g}^{R}	287	E_{g}^{R}	282	A_{1u}
1245	E_{g}^{R}	482	T_{2u}			289	T_{2u}	283	E_{g}^{R}
1250	T_{2g}^{R}	485	T_{2g}^{R}	488/490	T_{2g}^{R}	290	T_{2g}^{R}	284	T_{2u}

man scattering spectra, at 200 cm^{-1} the relative intensity of the T_{2g} mode is correctly reproduced in comparison to other peaks but at low frequency we have two peaks with the same intensity.

The carbon spectra are significantly different from those of silicon or germanium networks: for C-34 only one mode A_{1g} should present a significant active frequency, in parallel measurement. In contrast a perpendicular mea-

TABLE VI. Frequencies (in cm^{-1}) and symmetries of the vibrational modes in $\mathbf{\Gamma}$ for *X*-46 systems.

C-46		Si-46				Ge-46			
$\omega_{q,\nu}$	Sym.	$\omega_{q,\nu}$	Sym.	Theo. (Ref. 42)		$\omega_{q,\nu}$	Sym.	Theo. (Ref. 34)	
0	T_{1u}^{IR}	0	T_{1u}^{IR}	0	T_{1u}^{IR}	0	T_{1u}^{IR}	0	T_{1u}^{IR}
457	T_{2g}^{R}	114	T_{2g}^{R}	114	T_{2g}^{R}	65	T_{2g}^{R}	62	T_{2g}^{R}
505	T_{1g}	120	T_{1g}	126	T_{1g}	70	T_{1g}	63	T_{1g}
576	T_{2u}	129	A_{2u}	143	T_{2u}	76	A_{2u}	67	E_{g}^{R}
588	E_{g}^{R}	140	T_{1g}	144	T_{1u}^{IR}	79	T_{1g}	69	T_{1u}^{IR}
591	T_{1u}^{IR}	140	T_{2u}	157	T_{1g}	81	T_{2u}	71	T_{2u}
623	A_{2u}	143	T_{1u}^{IR}	164	T_{1u}^{IR}	82	T_{1u}^{IR}	74	T_{1g}
623	T_{1g}	147	E_{g}^{R}	172	E_{g}^{R}	82	E_{g}^{R}	77	T_{2g}^{R}
637	A_{2g}	153	E_{u}	182	E_{u}	86	E_{u}	78	A_{2u}
682	T_{2u}	166	T_{1g}	194	T_{2u}	93	T_{1g}	79	A_{2g}
695	E_{u}	169	T_{2u}	197	T_{1g}	93	A_{2g}	82	E_{u}
716	E_{g}^{R}	170	T_{2g}^{R}	198	T_{2g}^{R}	94	T_{2g}^{R}	83	T_{1g}
732	T_{1g}	173	T_{1u}^{IR}	208	T_{1u}^{IR}	94	T_{2u}	89	T_{1u}^{IR}
752	T_{2g}^{R}	175	A_{2g}	220	E_{u}	96	T_{2g}^{R}	89	T_{2g}^{R}
781	T_{1u}^{IR}	178	T_{2g}^{R}	224	E_{g}^{R}	96	T_{1g}	89	T_{1g}
818	T_{2u}	178	E_{u}	225	A_{2g}	96	T_{1u}^{IR}	89	T_{2u}
824	E_{g}^{R}	180	T_{1g}	236	T_{2g}^{R}	97	E_{u}	91	E_{u}
851	E_{u}	194	T_{1u}^{IR}	237	T_{1g}	103	T_{1u}^{IR}	93	T_{1u}^{IR}
879	T_{2g}^{R}	223	E_{g}^{R}	240	A_{2g}	131	E_{g}^{R}	131	E_{g}^{R}
878	A_{2g}	239	A_{2g}	246	T_{2u}	138	A_{2g}	138	T_{2u}
882	T_{1u}^{IR}	247	T_{2u}	250	T_{1u}^{IR}	142	T_{2u}	139	A_{2g}
909	T_{1g}	301	T_{1u}^{IR}	307	E_{g}	176	E_{g}^{R}	170	E_{g}^{R}
920	T_{2g}^{R}	303	E_{g}^{R}	309	T_{1u}^{IR}	177	T_{1u}^{IR}	172	T_{1u}^{IR}
946	T_{1u}^{IR}	305	T_{2g}^{R}	314	T_{2g}^{R}	179	T_{2g}^{R}	176	T_{2g}^{R}
948	A_{1g}^{R}	325	T_{2u}	332	T_{2u}	190	T_{2u}	186	T_{2u}
955	A_{2g}	326	A_{1u}	345	A_{1g}^{R}	193	A_{1u}	189	A_{1g}^{R}
992	T_{2u}	334	A_{1g}^{R}	349	A_{1u}	195	A_{1g}^{R}	190	A_{1u}
1007	T_{1u}^{IR}	355	T_{1g}	372	T_{1g}	209	T_{1g}	206	T_{1g}
1015	A_{1u}	370	T_{2u}	390	T_{2u}	217	T_{2u}	212	T_{2u}
1025	T_{2u}	375	T_{1u}^{IR}	393	T_{1u}^{IR}	220	T_{1u}^{IR}	215	T_{1u}^{IR}
1033	T_{1g}	383	A_{2g}	403	A_{2g}	223	A_{2g}	218	A_{2g}
1055	T_{1u}^{IR}	384	A_{2u}	409	A_{2u}	226	A_{2u}	223	A_{2u}
1058	A_{1g}^{R}	408	T_{2g}^{R}	423	E_{g}^{R}	240	T_{2g}^{R}	235	T_{1u}^{IR}
1062	E_{g}^{R}	414	E_{g}^{R}	429	T_{2u}	242	T_{1u}^{IR}	235	T_{2g}^{R}
1075	T_{1g}	418	T_{1u}^{IR}	431	T_{2g}^{R}	242	E_{g}^{R}	238	E_{g}^{R}
1082	T_{2u}	418	T_{1g}	441	T_{1g}	245	T_{1g}	240	T_{1g}
1088	T_{2g}^{R}	432	A_{1g}^{R}	445	A_{1g}^{R}	251	A_{1g}^{R}	247	A_{1g}^{R}
1088	T_{1u}^{IR}	442	T_{2u}	467	T_{2u}	260	T_{2u}	258	T_{2u}
1092	E_{g}^{R}	450	T_{1u}^{IR}	483	T_{1u}^{IR}	268	T_{1u}^{IR}	263	T_{1u}^{IR}
1129	A_{2u}	459	E_{g}^{R}	484	E_{g}^{R}	272	E_{g}^{R}	268	E_{g}^{R}
1140	T_{2u}	461	T_{2u}	489	T_{2u}	274	T_{2u}	271	T_{2u}
1143	E_{u}	462	E_{u}	492	T_{1u}^{IR}	275	E_{u}	272	T_{1g}
1152	A_{2g}	465	T_{1u}^{IR}	493	A_{2g}	277	T_{1u}^{IR}	272	T_{2g}^{R}
1158	T_{2g}^{R}	466	T_{2g}^{R}	495	T_{2u}	277	E_{u}	272	T_{1u}^{IR}
1167	T_{1u}^{IR}	467	T_{2u}	495	T_{2u}	277	T_{2g}^{R}	273	T_{2u}
1170	E_{g}^{R}	467	E_{u}	498	E_{u}	278	T_{1u}^{IR}	273	E_{u}
1192	A_{1u}	468	T_{1g}	498	E_{g}	278	T_{2u}	275	T_{1u}^{IR}

TABLE VI. (*Continued.*)

C-46		Si-46				Ge-46			
$\omega_{q,\nu}$	Sym.	$\omega_{q,\nu}$	Sym.	Theo. (Ref. 42)		$\omega_{q,\nu}$	Sym.	Theo. (Ref. 34)	
1192	T_{1g}	468	T_{2g}^{R}	498	T_{2g}^{R}	278	T_{1g}	275	E_u
1198	E_u	469	T_{1u}^{IR}	498	T_{1g}	279	T_{2g}^{R}	275	E_g^{R}
1198	T_{2u}	470	E_g^{R}	500	T_{1u}^{IR}	279	E_g^{R}	276	T_{2g}^{R}
1201	T_{2g}^{R}	470	A_{1u}	504	E_u	279	A_{1u}	277	A_{1u}
1202	T_{1u}^{IR}	471	T_{1g}	504	T_{1g}	281	T_{1g}	278	T_{1g}
1220	T_{1g}	474	T_{2g}^{R}	505	T_{2g}^{R}	281	T_{2g}^{R}	278	T_{2g}^{R}
1223	E_g^{R}	479	T_{2u}	511	A_{1g}^{R}	284	E_g^{R}	279	E_g^{R}
1229	T_{2g}^{R}	480	E_g^{R}	512	A_{1u}	284	A_{2g}	279	A_{2g}
1260	T_{2u}	481	A_{2g}	515	T_{2g}^{R}	285	T_{2u}	282	T_{2u}
1260	A_{1g}^{R}	481	A_{1g}^{R}	516	T_{2u}	286	A_{1g}^{R}	282	A_{1g}^{R}

surement must show more signals (four groups of peaks). For C-46, we obtain a spectrum with six equivalent peaks.

3. Infrared spectra

We have calculated the infrared spectra from dynamical matrix, we have plotted it on the Fig. 5. Our results on silicon clathrates are in agreement with those published by Li *et al.*,[51] in spite of that the frequencies found by these authors are slightly shifted from ours. The infrared spectra are less sensitive to the element than Raman spectra. The spectra depend on the dynamical properties, which results from a strong similarity between systems.

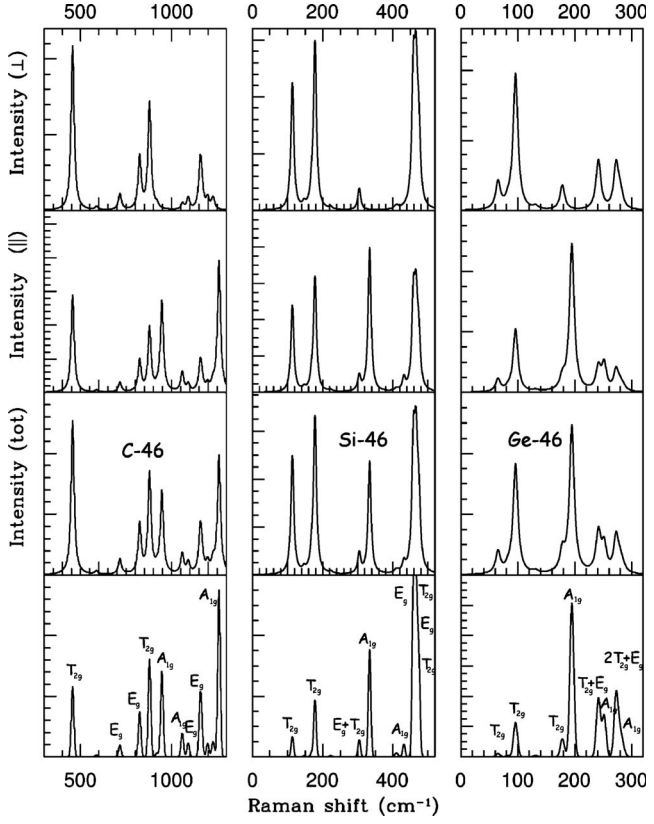

FIG. 3. Raman spectra of *X*-46 (from left to right: C, Si, and Ge) clathrates: from top to bottom figures: perpendicular, parallel, total Raman intensities, and total cross section convoluted with a uniform Gaussian broadening having 10–5 cm^{-1} width. We have used a damping constant $\Gamma_i = 10$ cm^{-1} for all modes. Peaks are labeled in function to their symmetries.

4. Polarizability and dielectric constants

Finally, we report the polarizability (α) and the permittivity (ϵ_∞) in Table VII. Quantitatively, dielectric constants are

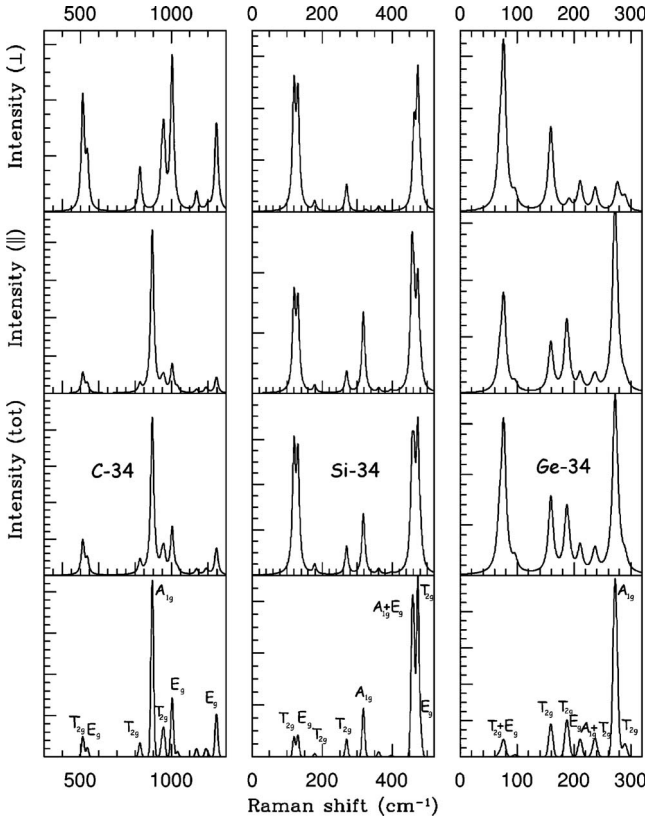

FIG. 4. Raman spectra of *X*-34 (from left to right: C, Si, and Ge) clathrates, see Fig. 3 for labels.

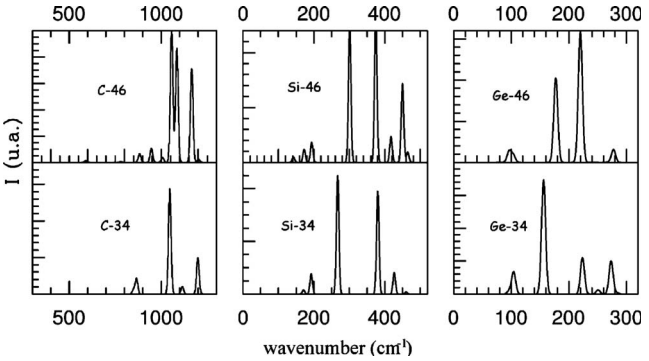

FIG. 5. Infrared spectra of *X*-46 and *X*-34 (from left to right: C, Si, and Ge) clathrates.

in agreement with the values found by Blase[17] within a GW approximation. The polarizability is lighter greater in clathrates than in diamond, and the Born effective charge is small (less <0.1 for Born charges) as in diamond phases, which accounts for the lack of LO-TO splitting.

B. Thermodynamical properties

The thermodynamical properties of clathrates and diamonds under pressure and temperature have been investigated from the interatomic constants. To compute these properties, two approaches for comparison were performed: the static approximation and the quasiharmonic approximation (QHA). Only carbon systems have been studied within the framework of the QHA.

1. Static approximation

This approximation consists of a calculation of the vibrational free energy (F_{vib}) at the optimized lattice parameter, where the effect of the temperature on the lattice parameter is neglected. The Helmholtz free energy, for nonmetallic systems, is then given by

$$F(T) = U_o + F_{\mathrm{vib}}(T), \tag{3}$$

where U_o is the internal energy of the cell at the optimized volume and

$$F_{\mathrm{vib}}(T) = k_B T \sum_{\mathbf{q},\nu} \ln[2\ \sinh(\xi_{\mathbf{q},\nu})] \tag{4}$$

the vibrational free energy ($\xi_{\mathbf{q},\nu}=\hbar\omega_{\mathbf{q},\nu}/2k_BT$). The summation on the vibration frequencies has been performed on $20\times20\times20$ tetrahedron grids. The heat capacity and the entropy have been evaluated following the relations:

TABLE VII. Dielectric constants (ϵ_∞) and polarizabilities $\vec{\vec{\alpha}} = \alpha\vec{\vec{I}}$ (in Å^3/atom).

	ϵ_∞	α
C-2	5.7 (5.5[a])	0.84
C-34	4.8 (4.7[b])	0.86
C-46	4.9	0.87
Si-2	13.6 (11.7[a])	3.73
Si-34	10.0 (9.8[b])	4.06
Si-46	10.4	4.03
Ge-2	18.3 (15.8[a])	4.40
Ge-34	12.4	4.67
Ge-46	12.8	4.65

[a]Experiment (Ref. 31).
[b]Theory GW calculations, Ref. 17.

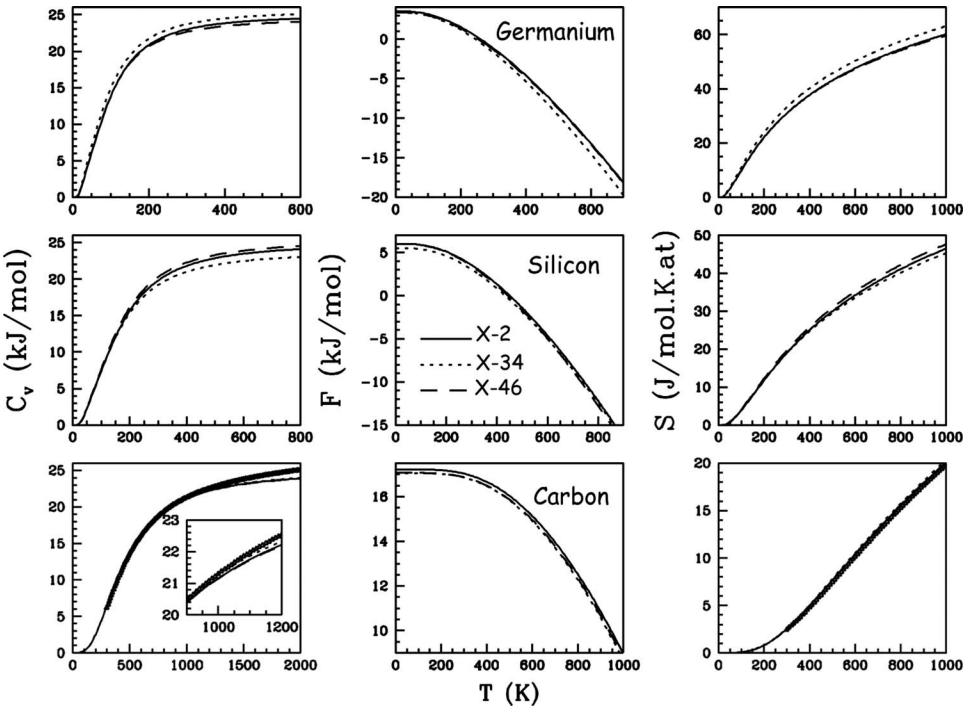

FIG. 6. Variation in the heat capacity (C_v), free energy (F), and entropy (S) in clathrates and diamond in the static approximation, from bottom to top: carbon, silicon, and germanium systems. Dots represent the experimental points (C_p, and S) of carbon diamond (Ref. 52).

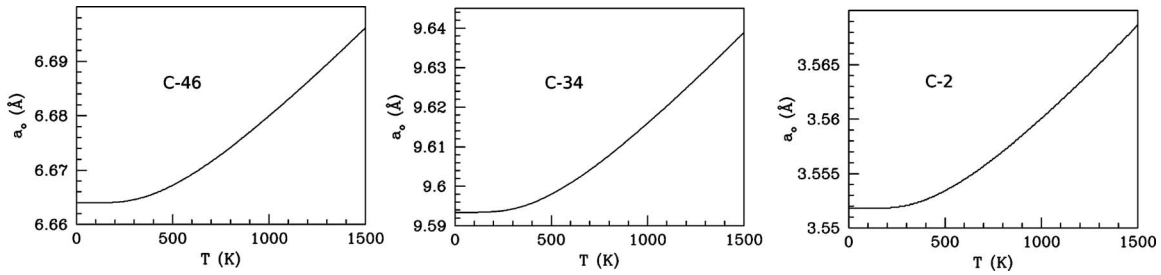

FIG. 7. Variation in the lattice parameter with respect to the temperature at 0 GPa.

$$C_v(T) = -T\frac{d^2F_{\text{vib}}}{dT^2} = -k_B\sum_{\mathbf{q},\nu}\left[\frac{\xi_{\mathbf{q},\nu}}{\sinh(\xi_{\mathbf{q},\nu})}\right]^2, \tag{5a}$$

$$S(T) = S_{\text{vib}}(T) = -\frac{dF_{\text{vib}}}{dT}. \tag{5b}$$

S, C_v, and F are plotted Fig. 6 for C, Si, and Ge systems, and compared with experimental data (C_p and S) for carbon diamond.[52] Until around 800 K, the static approximation reproduces accurately the heat capacity and entropy of carbon diamond. The results, reported for Si/Ge clathrates are in good agreement with those published by Biswas[53] and Tang.[41] In conclusion, according to the static approximation, diamond and clathrates behavior are, for a given element, slightly different.

2. QHA

If the anharmonic effects are neglected at the level of the QHA, the thermal expansion is restored by introducing the (anharmonic) effect of the temperature and the pressure on lattice parameters and thermodynamic properties in the Eq. (3). Isothermal fourth-order Birch-Murnaghan binding energy relation has been used to fit the free energy

$$F(a,T) = F_o + \frac{9}{8}B_oV_ou^2 + Au^3 + Cu^4 + \mathcal{O}[u^5], \tag{6}$$

where $u=(V_o/V)^{2/3}-1$. For a given temperature, the free energy has been fitted by a *spline*-type approximation. The pressure is then deduced from the following relation:

$$P(T,V) = -\left.\frac{\partial F(T,V)}{\partial V}\right|_T. \tag{7}$$

$V(T,P)$ is thus interpolated from $P(T,V)$, the Gibbs energy $G(T,P)$ is computed as the function of the pressure and temperature. The thermal dilatation coefficient and the Grüneisen parameter are deduced from

$$\alpha_v(T,P) = \frac{1}{V}\left.\frac{\partial V}{\partial T}\right|_P, \tag{8}$$

$$\gamma(T,P) = VB_o\alpha/C_v \tag{9}$$

while the heat capacity C_p and $C_v=\partial U/\partial T$ are linked by

$$C_p(T,P) = C_v + \alpha_v^2B_oVT. \tag{10}$$

To calculate F_{vib} we have restricted the summation on q points at the only $\mathbf{\Gamma}$ point for carbon systems. The temperature dependence of the lattice parameter and thermal expansion, respectively, are plotted in Figs. 7 and 8 up to 1500 K at 0 GPa. The P-V-T relationship of diamond and clathrates is reported in Fig. 9 for two temperatures.

The pressure and temperature behavior of C_p, C_v, and α of the three systems are very similar (Fig. 10). Differences occur at high pressure (up to 150 GPa), where the lattice parameter of C-46 is reduced contrary to C-34 and C-2, for which the related reduction occurs at higher pressure (around 700 GPa).[54] The Grüneisen parameters of Raman modes $[\gamma_i=-\frac{\partial \ln(\omega_i)}{\partial \ln(V)}]$ have been calculated and reported in Table VIII. For carbon diamond one found $\gamma=1.01$ for the Raman active mode at 1307 cm^{-1}, in agreement with experimental measurement.[55] Contrary to Si-34,[41] all Grüneisen parameters of carbon clathrates are positive. The Debye temperatures (θ_D), of clathrates, calculated and reported in Table IX, are 10% smaller than the diamond temperature.

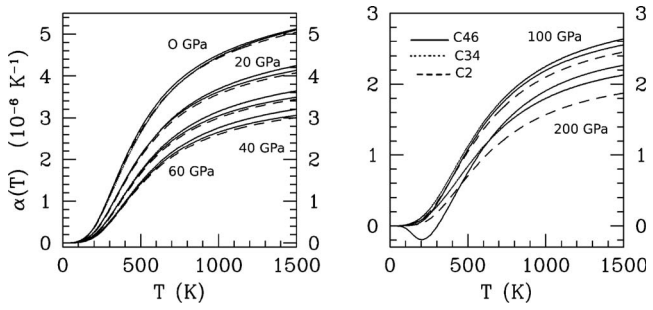

FIG. 8. Variation in the linear thermal $\alpha(T)$ for C-2 (dots), C-46 (line), and C-34 (dashed lines) with the temperature for different pressures: $0<P<60$ GPa (left), and 100, 200 GPa (right).

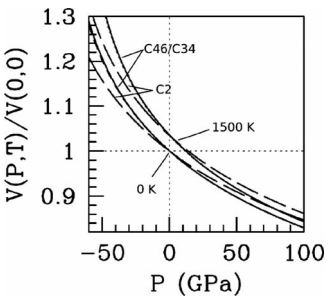

FIG. 9. Calculated P-V-T relationship of diamond and clathrates for two temperatures (0 K and 1500 K) taken as reference the volume at 0 K and 0 GPa.

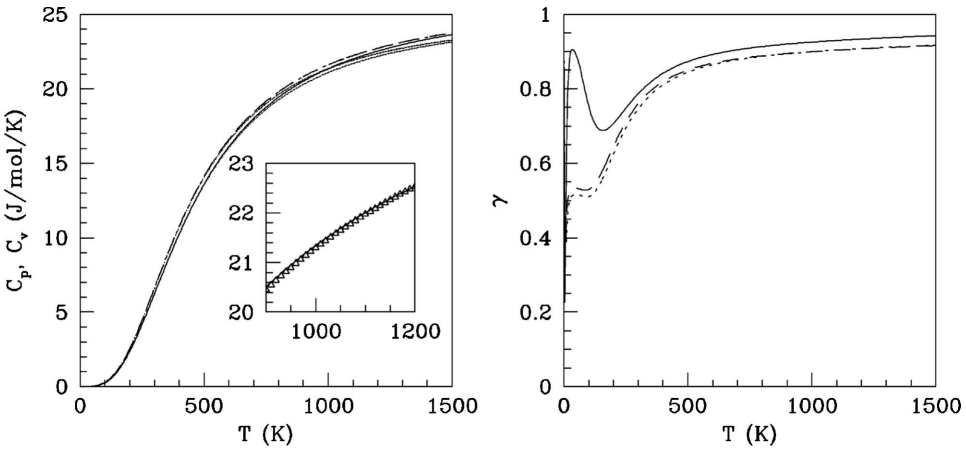

FIG. 10. Variation in the heat capacity (C_v and C_p) and Grüneisen parameter $[\gamma = \partial \ln(\Theta)/\partial \ln(V)]$ at 0 GPa. We have enlarged around 1000 K experimental and theoretical C_p of carbon diamond (dots represent experimental data (Ref. 52), dashed lines simulations).

C. (P,T) Phase diagram

We have investigated the phase diagram of carbon phases, by assuming the same Gibbs energies for carbon diamond with carbon clathrates, the temperature of the transition for a pressure. Figure 11 shows the phase diagram from 0 to 1500 K. At 0 K,the transition pressures P_t are −21 and −28 GPa for C-46 and C-34, respectively. These negative pressures agree with those calculated by Perottoni *et al.*[13]

TABLE VIII. Calculated Raman frequencies (ω_i) and Grüneisen parameters $[\gamma_i = -\partial \ln(\omega_i)/\partial \ln(V)]$ for C-34 and C-46.

C-34		C-46	
ω_i (cm^{-1})	γ_i	ω_i (cm^{-1})	γ_i
	E_g		
538	0.52	588	0.76
958	1.14	716	1.01
1137	1.24	824	1.49
1245	1.17	1062	1.44
		1092	1.62
		1170	1.22
		1223	0.88
	A_{1g}		
894	1.59	948	1.18
1032	1.11	1058	1.75
1189	0.80	1260	1.02
	T_{2g}		
513	0.26	457	0.48
827	1.19	752	0.60
913	0.35	879	0.49
947	1.22	920	0.93
1003	1.32	1088	1.05
1175	1.36	1158	1.20
1200	0.96	1201	0.97
1250	0.97	1229	0.99

(using a Hartree-Fock approximation), and Rey *et al.*[16]

Gibbs' phase rule for one component system shows that two phases coexist along a curve in the T,P plane, where the Clausius-Clapeyron equation $(dP_t/dT = \Delta S/\Delta V)$ is the coexistence curve. We found $dP_t/dT > 0$ for C-46/C2 and C-34/C2. Negative pressure values are expected in those kinds of transitions implying expanded phases compared to diamond. In absolute values, the transition pressures are found much larger than those calculated for Si-2/Si-46 (−6 GPa) and Ge-2/Ge-46 (−2.4 GPa).

D. Elasticity

The elastic constants (C_{ij}) have been derived from vibrational acoustic dispersion slopes presented above. In cubic systems, the elastic tensor can be described by three independent elastic constants (see Ref. 31): namely, C_{11}, C_{12}, and C_{44}. The slope of the acoustic branches along the [100] direction are related to C_{11} and C_{44}

$$v_l^{[100]} = \sqrt{\frac{C_{11}}{\rho}}, v_t^{[100]} = \sqrt{\frac{C_{44}}{\rho}}, \tag{11a}$$

where $v_l^{[100]}$ and $v_t^{[100]}$ are, respectively, the longitudinal and transverse velocities of the sound and ρ the density. For C_{12}, we use the [111] direction: $v_l^{[111]} = \sqrt{\frac{C_{11}+2C_{12}+4C_{44}}{3\rho}}$.

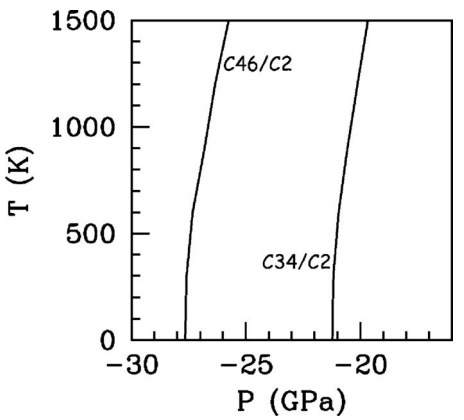

FIG. 11. Equilibrium phase diagram (P,T) of carbon diamond and clathrates.

TABLE IX. The densities (in kg/m^3), the elastic constants (in GPa), the bulk modulus (in GPa), the factors of anisotropy C_a, the shears moduli G (in GPa), the Young modulus Y along the [100] direction (in GPa), the Poisson ratio ν, the Young modulus along the [111] direction (in GPa), and the Debye temperatures (in K) for each system.

	ρ	C_{11}	C_{12}	C_{44}	B_o	C_a	G	Y_{100}	ν	Y_{111}	θ_D
C-2	3593	1092 (1076[a])	135 (125[a])	585 (576[a])	458	0.81	475	1060	0.11	1231	2230
C-34	3098	966	87	437	381	0.99	439	952	0.08	947	2083
C-46	3129	935 (960[b])	127 (117[b])	462 (472[b])	396	0.87	403	903	0.11	996	1996
Si-2	2381	167 (166[a])	63 (64[a])	78 (79[a])	103	0.62	48	125	0.30	185	555
Si-34	2074	135 (137[c])	55 (57[c])	44 (39[c])	82	0.92	40	103	0.29	111	516
Si-46	2098	140 (135[c])	47 (58[c])	47 (40[c])	78	0.97	46	116	0.25	118	551
Ge-2	5566	134 (130[a])	54 (48[a])	66 (68[a])	82	0.59	39	102	0.29	156	315
Ge-34	4902	114	46	36	69	0.94	34	88	0.29	92	301
Ge-46	4953	115	37	40	63	0.96	39	97	0.24	101	320

[a]Experiment, Ref. 31.
[b]Theory, Ref. 19.
[c]Theory, Ref. 33.

For diamond, simulations reproduce with accuracy experimental data (see Table IX). The differences for clathrates between previous calculations of elastic constants and ours simulations are small. The elastic constants of clathrates are always smaller (10–20 %) than diamond analogs.

From elastic constants, experimental sets of parameters such the bulk modulus B_o, the factor of anisotropy C_a, the shear modulus G, and the Young's modulus Y along two main crystallographic directions ([100] and [111]) can be deduced according to the following relations (see Table IX):

$$B_o = \frac{C_{11} + 2C_{12}}{3}, \tag{12a}$$

$$C_a = \frac{C_{11} - C_{12}}{2C_{44}}, \tag{12b}$$

$$G = \frac{C_{11} - C_{12}}{2}, \tag{12c}$$

$$Y_{100} = \frac{(C_{11} + 2C_{12})(C_{11} - C_{12})}{C_{11} + C_{12}}, \tag{12d}$$

$$\frac{1}{Y_{111}} = \frac{1}{Y_{100}} + \frac{C_{11} - C_{12} - 2C_{44}}{3C_{44}(C_{11} - C_{12})}. \tag{12e}$$

One can first note that B_o calculated from a Murnaghan fit (see Table II) and from elastic constants (Table IX) are very close. The factor of anisotropy is close to 1 in clathrates, indicating that they can be viewed as strongly isotropic systems according to strains. The Poisson's ratio ν, which quantifies the stability of a crystal against shear, are considerably smaller for carbon systems than for the other silicon/germanium systems, which suggests that carbon clathrates should be relatively stable against shear. To conclude, one found that the Young's Modulus vary little in function to the crystallographic direction. These results could explain the good stability of clathrates under pressure.

VI. CONCLUSION

We have reported first-principles study of free guest carbon clathrates properties C-34 and C-46, and compared them with silicon and germanium clathrates and diamond analogs. In spite of a similar sp^3 hybridization for the nine systems, we have shown that the lack of p core states in carbon materials induces strong modification in vibrational properties comparatively to Si and Ge. The pentagonal rings provide additional strong changes in electronic and vibrational properties.

The study of electronic states around the band gap shows a slight dependency on the element, which results in the same optical properties in silicon and carbon clathrates. We have shown that the vibrational properties of carbon phases differ from their Si/Ge analog structures, whereas vibrational properties of Si and Ge systems can be relied through their atomic weight ratio. Raman and infrared spectra are displayed for an upcoming suitable experimental analysis. Thermodynamical properties (S, F, C_v) are revealing to be less altered by crystallographic effect and that for a given element it is difficult to separate behaviors. It is only at high pressure that the evolution of lattice parameters of clathrates differs from diamond. The phase diagram calculated is found to be compatible with previous estimations. We conclude the paper with a presentation of elastic properties computed from acoustic slopes.

ACKNOWLEDGMENTS

Calculations have been performed at supercomputer facilities at *Calmip* CICT Toulouse (France). D.C. is indebted to P. Demont and D. Monceau for a critical reading of the manuscript.

*damien.connetable@ensiacet.fr

[1] J. L. Cohn, G. S. Nolas, V. Fessatidis, T. H. Metcalf, and G. A. Slack, Phys. Rev. Lett. **82**, 779 (1999).
[2] J. S. Tse, K. Uehara, R. Rousseau, A. Ker, C. I. Ratcliffe, M. A. White, and G. MacKay, Phys. Rev. Lett. **85**, 114 (2000).
[3] L. Qiu, M. A. White, Z. Li, J. S. Tse, C. I. Ratcliffe, C. A. Tulk, J. Dong, and O. F. Sankey, Phys. Rev. B **64**, 024303 (2001).
[4] G. S. Nolas, J.-M. Ward, J. Gryko, L. Qiu, and M. A. White, Phys. Rev. B **64**, 153201 (2001).
[5] D. Connétable, V. Timoshevskii, E. Artacho, and X. Blase, Phys. Rev. Lett. **87**, 206405 (2001).
[6] G. Benedek, M. Bernasconi, and A. Gambirasio, Phys. Status Solidi B **237**, 296 (2003).
[7] M. Bernasconi, S. Gaito, and G. Benedek, Phys. Rev. B **61**, 12689 (2000).
[8] D. Connétable, Phys. Rev. B **75**, 125202 (2007).
[9] H. Kawaji, H. O. Horie, S. Yamanaka, and M. Ishikawa, Phys. Rev. Lett. **74**, 1427 (1995).
[10] D. Connétable, V. Timoshevskii, B. Masenelli, J. Beille, J. Marcus, B. Barbara, A. M. Saitta, G.-M. Rignanese, P. Mélinon, S. Yamanaka, and X. Blase, Phys. Rev. Lett. **91**, 247001 (2003).
[11] A. San-Miguel, P. Kéghélian, X. Blase, P. Mélinon, A. Perez, J. P. Itié, A. Polian, E. Reny, C. Cros, and M. Pouchard, Phys. Rev. Lett. **83**, 5290 (1999).
[12] G. B. Adams, M. O'Keeffe, A. A. Demkov, O. F. Sankey, and Y.-M. Huang, Phys. Rev. B **49**, 8048 (1994).
[13] C. A. Perottoni and J. A. H. da Jornada, J. Phys.: Condens. Matter **13**, 5981 (2001).
[14] R. Nesper, K. Vogel, and P. E. Blöchl, Angew. Chem. **32**, 701 (1993).
[15] G. Benedek and L. Colombo, Mater. Sci. Forum **232**, 247 (1996); I. Spagnolatti, M. Bernasconi, and G. Benedek, Eur. Phys. J. B **34**, 63 (2003).
[16] N. Rey, A. Munoz, P. Rodriguez-Hernández, and A. San-Miguel, J. Phys.: Condens. Matter **20**, 215218 (2008).
[17] X. Blase, Phys. Rev. B **67**, 035211 (2003).
[18] D. Connétable and X. Blase, Appl. Surf. Sci. **226**, 289 (2004).
[19] X. Blase, P. Gillet, A. San Miguel, and P. Melinon, Phys. Rev. Lett. **92**, 215505 (2004).
[20] F. Zipoli, M. Bernasconi, and G. Benedek, Phys. Rev. B **74**, 205408 (2006).
[21] A. San-Miguel and P. Toulemonde, High Press. Res. **25**, 159 (2005).
[22] P. Mélinon, P. Kéghélian, X. Blase, J. Le Brusc, A. Perez, E. Reny, C. Cros, and M. Pouchard, Phys. Rev. B **58**, 12590 (1998).
[23] P. Giannozzi, S. Baroni, N. Bonini, M. Calandra, R. Car, C. Cavazzoni, D. Ceresoli, G. L. Chiarotti, M. Cococcioni, I. Dabo, A. Dal Corso, S. Fabris, G. Fratesi, S. de Gironcoli, R. Gebauer, U. Gerstmann, C. Gougoussis, A. Kokalj, M. Lazzeri, L. Martin-Samos, N. Marzari, F. Mauri, R. Mazzarello, S. Paolini, A. Pasquarello, L. Paulatto, C. Sbraccia, S. Scandolo, G. Sclauzero, A. P. Seitsonen, A. Smogunov, P. Umari, and R. M. Wentzcovitch, J. Phys.: Condens. Matter **21**, 395502 (2009).
[24] J. P. Perdew and A. Zunger, Phys. Rev. B **23**, 5048 (1981).
[25] D. M. Ceperley and B. J. Alder, Phys. Rev. Lett. **45**, 566 (1980).
[26] N. Troullier and J. L. Martins, Phys. Rev. B **43**, 1993 (1991); Solid State Commun. **74**, 613 (1990).
[27] L. Kleinman and D. M. Bylander, Phys. Rev. Lett. **48**, 1425 (1982).
[28] H. J. Monkhorst and J. D. Pack, Phys. Rev. B **13**, 5188 (1976).
[29] S. Baroni and R. Resta, Phys. Rev. B **33**, 7017 (1986).
[30] S. Baroni, P. Giannozzi, and A. Testa, Phys. Rev. Lett. **58**, 1861 (1987).
[31] C. Kittel, *Introduction to Solid State Physics* (Wiley, New York, 1996).
[32] G. S. Nolas, M. Beekman, J. Gryko, G. A. Lamberton, T. M. Tritt, and P. F. McMillan, Appl. Phys. Lett. **82**, 910 (2003).
[33] K. Moriguchi, S. Munetoh, A. Shintani, and T. Motooka, Phys. Rev. B **64**, 195409 (2001).
[34] J. Dong and O. F. Sankey, J. Phys.: Condens. Matter **11**, 6129 (1999).
[35] A. M. Guloy, R. Ramlau, Z. Tang, W. Schnelle, M. Baitinger, and Y. Grin, Nature (London) **443**, 320 (2006).
[36] K. Moriguchi, S. Munetoh, and A. Shintani, Phys. Rev. B **62**, 7138 (2000).
[37] F. D. Murnaghan, Proc. Natl. Acad. Sci. U.S.A. **30**, 244 (1944).
[38] J. Gryko, P. F. McMillan, R. F. Marzke, G. K. Ramachandran, D. Patton, S. K. Deb, and O. F. Sankey, Phys. Rev. B **62**, R7707 (2000).
[39] J. Zhao, A. Buldum, J. P. Lu, and C. Y. Fong, Phys. Rev. B **60**, 14177 (1999).
[40] G. S. Nolas, C. A. Kendziora, J. Gryko, J. Dong, C. W. Myles, A. Poddar, and O. F. Sankey, J. Appl. Phys. **92**, 7225 (2002).
[41] X. Tang, J. Dong, P. Hutchins, O. Shebanova, J. Gryko, P. Barnes, J. K. Cockroft, M. Vickers, and P. F. McMillan, Phys. Rev. B **74**, 014109 (2006).
[42] M. Menon, E. Richter, and K. R. Subbaswamy, Phys. Rev. B **56**, 12290 (1997).
[43] D. L. Rousseau, R. P. Bauman, and S. P. S. Porto, J. Raman Spectrosc. **10**, 253 (1981).
[44] Y. Guyot, B. Champagnon, E. Reny, C. Cros, M. Pouchard, P. Melinon, A. Perez, and I. Gregora, Phys. Rev. B **57**, R9475 (1998).
[45] It is interesting to note that vibrational properties of tin clathrates can too be deduced from germanium thanks a atomic weight ratio with a good accuracy.
[46] P. Giannozzi, S. de Gironcoli, P. Pavone, and S. Baroni, Phys. Rev. B **43**, 7231 (1991).
[47] P. Pavone, K. Karch, O. Schütt, W. Windl, D. Strauch, P. Giannozzi, and S. Baroni, Phys. Rev. B **48**, 3156 (1993).
[48] M. Lazzeri and F. Mauri, Phys. Rev. Lett. **90**, 036401 (2003).
[49] D. Porezag and M. R. Pederson, Phys. Rev. B **54**, 7830 (1996).
[50] J. Dong, O. F. Sankey, and G. Kern, Phys. Rev. B **60**, 950 (1999).
[51] J. C. Li, C. L. Wang, W. X. Wang, H. Peng, R. Z. Zhang, M. L. Zhao, J. Liu, J. L. Zhang, and L. M. Mei, J. Appl. Phys. **105**, 043503 (2009).
[52] G. A. Slack and S. F. Bartram, J. Appl. Phys. **46**, 89 (1975).
[53] K. Biswas, C. W. Myles, M. Sanati, and G. S. Nolas, J. Appl. Phys. **104**, 033535 (2008).
[54] J. Xie, S. P. Chen, J. S. Tse, S. de Gironcoli, and S. Baroni, Phys. Rev. B **60**, 9444 (1999).
[55] B. B. Pate, I. Lindau, and W. E. Spicer, in *Proceedings of the 17th International Conference on the Physics of Semiconductors*, San Francisco, 1984, edited by J. D. Chadi and W. A. Harrison (Springer-Verlag, New York, 1985), p. 1181.